Journal of Materials Chemistry B

PAPER

View Article Online
View Journal | View Issue

Cite this: J. Mater. Chem. B, 2018, 6, 1335

Sinapultide-loaded lipid microbubbles and the stabilization effect of sinapultide on the shells of lipid microbubbles†

Dong Liu,‡[ab] Zuoheng Zhang,‡[a] Zhiguo Qin,[a] Jing Xing,[a] Yang Liu,[a] Juan Jin,[a] Fang Yang *[a] and Ning Gu *[a]

Received 25th October 2017,
Accepted 16th January 2018

DOI: 10.1039/c7tb02799k

rsc.li/materials-b

Microbubbles (MBs) hold promise in various biomedical applications due to their ultrasound-responsive properties. However, the stability and contrast enhancement duration of gas encapsulated MBs are still challenging. The aim of this study is to fabricate novel sinapultide (a synthetic pulmonary surfactant) stabilized MBs as ultrasound contrast agents. The optimized MBs generated from a mixture of phospholipid components and sinapultide have an average diameter of 1.82 ± 0.15 μm and a zeta potential of −55.2 ± 3.9 mV. Over 95% of the MBs have a mean diameter of less than 8 μm, indicating that the appropriately sized MBs can be applied as ultrasound contrast agents used in clinic. Furthermore, the interaction between sinapultide and lipid molecules and the stabilization mechanism of sinapultide on the shells of MBs were investigated by molecular dynamics simulation. The results demonstrate that the stability of MBs was increased effectively when the appropriate amount of sinapultide was added due to the decrease of surface tension. Accordingly, acoustic accumulation imaging analysis *in vitro* indicates that stable gas encapsulated sinapultide loaded MBs can provide a high scattering intensity resulting in better echogenicity. And the optimized concentration of sinapultide-loaded MBs can improve the contrast enhancement effect obviously compared with non-sinapultide MBs. Therefore, sinapultide-loaded lipid MBs may be designed as novel ultrasound contrast agents and used for clinical application in the future.

1 Introduction

Gas-filled microbubbles (MBs) have been widely used as ultrasound contrast agents (UCAs) in biomedical applications.[1–3] Doppler signals from small and/or deep-lying vessels are enhanced and the difference in echo texture between normal and adjacent abnormal tissues can be further increased by UCAs.[4,5] Compared with radioactive diagnosis, ultrasonic imaging has been considered as a promising diagnostic tool due to the advantages of non-invasiveness, real-time detection, convenient use, cost-efficiency, and better biological safety.[6–8] Apart from their use in diagnosis, gas-filled MBs have also attracted more and more attention due to their excellent potentiality as ultrasound-mediated drug and gene delivery systems.[8–10] Therefore, novel UCAs for applications in ultrasound medicine and drug delivery hold great promise.

Typical MBs used as UCAs are commonly prepared by various methods including sonication,[11] emulsification,[12] microfluidic approaches,[13] inkjet printing[14] and coaxial electrohydrodynamic atomization.[15] Conventionally, they are composed of gaseous cores and stabilizing shells. An inert gas that is sparingly soluble in blood such as SF_6 or perfluorocarbon (PFC) is selected to substitute air as the gas component.[16] In order to stabilize MBs against gas dissolution and coalescence, their shell materials are elaborately designed. Nowadays, the proposed shell materials are always composed of lipids, polymers, proteins, and surfactants.[17–19] Among them, shells composed of lipids and surfactants offer excellent structural characteristics and acoustic responses.[20] Such MBs readily expand, compress, and rupture under ultrasound exposure. However, novel preparation techniques and shell materials still need to be developed in order to achieve better biosafety.[21]

Pulmonary surfactants (PSs) are complicated mixtures of lipids and proteins that cover the gas/liquid interface of lung bronchioles.[15] The main function of PSs lies in maintaining normal respiratory mechanics by reducing alveolar surface tension to prevent alveolar collapse.[22] Besides, they also play

[a] State Key Laboratory of Bioelectronics and Jiangsu Key Laboratory for Biomaterials and Devices, School of Biological Science and Medical Engineering, Southeast University, Nanjing, 210096, P. R. China. E-mail: yangfang2080@seu.edu.cn, guning@seu.edu.cn
[b] School of Biology and Pharmaceutical Engineering, West Anhui University, Lu'an, 237000, P. R. China

† Electronic supplementary information (ESI) available. See DOI: 10.1039/c7tb02799k

‡ These authors contributed equally to this work.

important roles in providing uniform lung inflation, improving the efficiency of airway clearance, and alleviating lung inflammatory reaction. At present, exogenous surfactants derived from animal and/or artificial synthesis are widely used as effective complementary therapeutic agents for neonatal respiratory distress syndrome (NRDS).[23–25] Apart from pure animal-derived extracts such as Curosurf® and Infasurf®, there are many other kinds of lung surfactant compositions on the market: for instance, partially synthetic PS formulations such as Survanta® and Surfactant-TA®, and chemically synthesized pure PS components like Surfaxin®.[26–29] In addition, PS-based microbubble formulations have also been developed. R. E. Pattle first discovered stable lung surfactant MBs derived from lung lavage fluids in 1955.[30] In the follow-up studies, researchers found that MBs prepared using animal-sourced lung surfactants could be used as ultrasound imaging contrast agents and drug delivery carriers due to their better stability.[31,32] However, the recent research progress mostly focus on lung surfactants derived from animals, in which safety issues like the risk of anaphylaxis remain a big challenge. Furthermore, the ratio of surface-active proteins to lipids was uncontrollable because the individual animal differences may be variable from batch to batch.[32] Therefore, novel surfactant preparations composed of essential surfactant protein analogs and synthetic phospholipids were developed to substitute animal-derived surfactants.[33] Surfaxin®, the first peptide-based synthetic pulmonary surfactant used in clinical application, was approved by the Food and Drug Administration (FDA) in 2012 for the treatment of NRDS. Sinapultide (KL4), a novel 21-amino-acid peptide, was used as a surfactant protein analog in the formulation to mimic the function of the critical human pulmonary surfactant protein (SP-B).[34–36] Compared with animal-derived pulmonary surfactants, such a synthetic surfactant has a higher biosafety and batch homogeneity. Therefore, in this study, based on the commonly used therapeutic surfactant replacement formulation, Surfaxin (Discovery Laboratories, Inc.), we developed novel sinapultide loaded lipid MBs, which were filled with sulfur hexafluoride (SF_6) in the core of MBs. First, stable synthetic pulmonary surfactant MBs in high yields were successfully prepared. Moreover, the effects of sinapultide concentration on acoustic imaging *in vitro* and the stabilization mechanism of sinapultide MBs were also investigated. The good stability, duration, and appropriate size distribution indicate that sinapultide loaded lipid MBs have the potential to be used as ultrasound contrast agents and pulmonary drug delivery systems in the future.

2 Experimental

2.1 Materials

Sinapultide (purity > 98%) was purchased from Paihepaide Pharmaceutical Technology Co., Ltd (Zhengzhou, China). Fluorescein isothiocyanate–sinapultide (FITC–sinapultide) (purity > 98%) was purchased from GenScript Biotechnology Co., Ltd (Nanjing, China). Dipalmitoylphosphatidylcholine (DPPC, purity >99%) was obtained from Southeast Pharmaceuticals Co., Ltd (Suzhou, China). Phosphatidylglycerol monosodium salt (POPG-Na, purity >99%) was purchased from Shanghai Advanced Vehicle Technology Co., Ltd (AVT, Shanghai, China). Palmitic acid (PA, purity >98%) and dioctadecyl-tetramethylindocarbocyanine perchlorate (DiI C_{18}, purity >98%) were purchased from Sigma-Aldrich Chemical Co. (St. Louis, MO, USA). Sulfur hexafluoride (SF_6) with a purity of 99.99% was obtained from Qiangyuan Gas Co., Ltd (Wuhu, China). All other solvents and reagents were of analytical purity.

2.2 Fabrication of microbubbles

Film dispersion and sonication methods were used to prepare sinapultide loaded lipid MBs.[37] Briefly, the optimized sinapultide loaded MB formulation was composed of 0.1 mg of sinapultide, 23.22 mg of DPPC, 7.68 mg of POPG-Na, and 4.21 mg of PA. The prescribed ingredients were synchronously dissolved in 2 mL of chloroform with ultrasound. Then, the organic solvent was evaporated under reduced pressure in a rotary evaporator for 2 h with a rotation speed of 110 rpm, and the water bath temperature was maintained at 25 °C. After all the organic solvent was removed from the mixture, a film was obtained upon drying the mixture at 30 °C in a vacuum oven for 12 h. Phosphate buffered saline (PBS, 1 mL, pH = 7.4 ± 0.1) was added to the sinapultide loaded lipid film in a round-bottom flask. After PBS was added to the flask, an ultrasonic water bath was carried for 15 minutes at 60 °C (30 kHz). And the precursor solutions for lipid-coated MBs were obtained. 1 mL aliquots of the precursor milk-white emulsion were placed in a 3 mL glass vial, and the vial was capped and sealed immediately.[31] The collected emulsion was stored at 4 °C in tightly capped vials sealed with paraffin films for filling gas.[38]

As SF_6 was required as the filling gas, the air headspace of the vial was replaced using a self-made gas exchange apparatus. MBs were produced using a homogenizer (Aoshen Instrument Co., Ltd, Bioprep-24, Hangzhou, China), and the vial was shaken at a speed of 4.0 m s^{-1} for 60 s. The shaking action brought the gas to the aqueous phase and a suspension of MBs was obtained. Control MBs without sinapultide were prepared using the same procedures as those mentioned above just without adding sinapultide. Furthermore, to optimize the ultrasound imaging enhancement of the prepared sinapultide loaded lipid MBs, we also performed formulation screening. Based on the fixed input amount of the gas and lipids, the concentrations of sinapultide were divided into five groups: 0.05, 0.1, 0.2, 0.4 and 0.8 mg mL^{-1}. To test the stability of the sinapultide microbubble formulation, a mother liquor of the sinapultide suspension was prepared as described above with a sinapultide concentration of 0.1 mg mL^{-1}. Before the sample was used, MBs were diluted to an appropriate concentration in PBS (pH = 7.4 ± 0.1), and all of them were prepared in parallel.

2.3 Sinapultide loading efficiency measurements

In order to measure the amount of sinapultide encapsulated in the MBs, the centrifugation method was used. 500 μL of sinapultide MBs for different prescriptions was dispersed in PBS (5 mL, pH 7.4 ± 0.1) initially by centrifuging at 3000 rpm

for 5 min in a syringe. Then the upper layer of foam was obtained, after which 2 mL of 60% acetonitrile/water was added to the separated MBs to destroy and dissolve the loaded sinapultide. After separation, the amount of sinapultide encapsulated in the MBs was measured by high performance liquid chromatography (HPLC) using a reversed-phase C_{18} column (250 mm × 4.6 mm, 5 μm particle size; DIKMA Corp., Beijing, China). The mobile phase conditions were an acetonitrile/water solution (60 : 40, v/v) with 0.1% trifluoroacetic acid (TFA) at 30 °C at a flow rate of 1.0 mL min^{-1}. The entrapment efficiency (EE) was calculated as:

$$EE\ (\%) = W_P/W_T \times 100\% \quad (1)$$

where W_P is the amount of sinapultide entrapped in MBs, and W_T is the total amount of sinapultide added to the solution.

The loading capacity (LC) (mass%) was calculated as:

$$LC\ (\%) = W_P/W_{MB} \times 100\% \quad (2)$$

where W_{MB} is the amount of MBs loaded with sinapultide.

2.4 Structural and physicochemical characterization

Samples in PBS solution were placed on glass slides and observed with an inverted microscope (Nikon, Eclipse TS100, Tokyo, Japan). The morphological structure of ultimately obtained MBs was further observed by transmission electron microscopy (TEM) (JEOL, JEM-2100EX, Tokyo, Japan) and scanning electron microscopy (SEM) (Carl Zeiss, Ultra-Plus, Oberkochen, Germany). The samples were dispersed on copper grids followed by negative staining with 2% phosphotungstic acid for TEM analysis. For SEM analysis, the sample solution was dispersed onto a silicon wafer and then dried at room temperature. For a more detailed view of the assembled structure of sinapultide on MBs, laser confocal scanning microscopy (LCSM) (Leica, TCS-SP8, Solms, Germany) was used to determine the morphology of DiI labelled MBs. The mean diameter of the bubbles was measured using a particle size analyser (Beckman Coulter, California, USA). The zeta potential of MBs was examined using a ZetaPALS instrument (Brookhaven Instruments Corporation, Austin, TX). The MBs for the zeta potential analysis were diluted with PBS (pH 7.4). Measurements were carried out at 25 ± 1 °C. Each sample was tested in triplicate.

2.5 *In vitro* ultrasound imaging evaluation

For acoustic imaging evaluation of sinapultide MBs *in vitro*, we used a laboratory made agar phantom with similar ultrasonic parameters to human soft tissue, which was composited with 3.1% agar, 92.7% distilled degassed water, and 4.2% glycerol. A round hole with a depth of 20 mm was prepared in the gel phantom to load samples. The testing samples were imaged using VisualSonics micro-imaging Vevo 2100 systems (FUJIFILM VisualSonics, Inc., USA) and a transducer of MS-250 was used. The transmit frequency was set at 18 MHz and the acquisition contrast gain was 35 dB. All parameters remained unchanged throughout the imaging process, and degassed water was tested to confirm a clear background signal before sampling. Then sinapultide MBs with different concentrations were injected into the gel phantom to be imaged. The mean power intensities under B-mode and contrast mode were analyzed in the Region of Interest (ROI).

2.6 Molecular dynamics simulations

In order to study the interaction between the sinapultide molecules and lipid agents, molecular dynamics simulation was applied. We used a coarse grained (CG) force field, MARTINI,[39,40] for larger length-scale and longer time-scale systems. In our system, two symmetric monolayers were at two vacuum–water interfaces. Each monolayer was constructed from 300 DPPC lipids and 92 POPG lipids according to the prescribed ratio in experiments (Table S1, ESI†). The POPG lipid contained a glycerol group (P4 bead) instead of a choline moiety (Q_0 bead) in DPPC (Fig. 1A and B).[41] Therefore, we replaced 184 water beads by cations (NA^+).[42] Sinapultide (KL4) was a synthetic product containing 21 amino acids.[43] Mapping of helical sinapultide was in line with new Martini forcefields (2.2).[44] We chose Qd beads for the positively charged Lys in the neutral pH system because the p*K* value of Lys was ~10.40.[45] Similarly, we also replaced the corresponding amount of water beads by anions. We ran 100 ns equilibrium simulation for DPPC and POPG bilayers and a sinapultide molecule (Fig. 1C) in bulk water to obtain an appropriate structure with lower energy.

Subsequently, 0, 2, 4, 8, 16 and 24 energy-optimized sinapultides were inserted into the interface between the water slab and each monolayer respectively. Then, we performed 400 ns equilibrium simulation for every system to relax any steric conflicts. We observed all of the sinapultides laid parallel to the polar head groups of the monolayer and were wrapped by lipids partially (Fig. 1D), which was consistent with previous experimental studies.[46,47] Finally, we used an *NVT* ensemble for our simulations. The *z*-direction scale of the box was kept constant, while the *x*/*y*-direction scale of the box was expanded and compressed at the same ratio. We obtained surface tensions under different monolayer areas and the critical areas where some lipid pores formed, which would simply illustrate the effects of the sinapultide concentration on the stability of the monolayer (DPPC/POPG).

All simulations were performed with a GROMACS 4.5.4 simulation package.[48] The cutoff of van der Waals interactions was 1.2 nm. In order to reduce the cutoff noise, both the Lennard-Jones potential and the Coulombic potential were smoothly shifted to zero between 0.9 nm and 1.2 nm. Lipids, water/neutralizing counterions and sinapultide were coupled separately to Berendsen heat baths at T = 300 K with a coupling

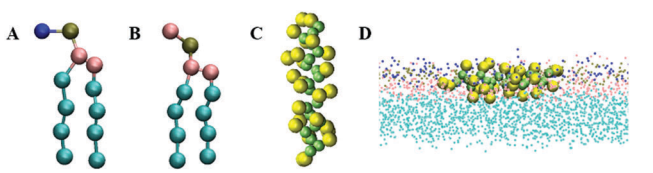

Fig. 1 Martini-based snapshots of DPPC (A) and POPG (B) molecules. Two molecules were composed of amine groups (blue), phosphate groups (brown), glycerol groups (pink) and carbon chains (cyan). (C) Snapshot of a coarse-grained sinapultide (KL4) including a helical backbone structure (green) and amino acid side chains (yellow). (D) Snapshot of a sinapultide wrapped by lipids partially on the monolayer.

constant τ = 1 ps. Berendsen coupling schemes for both pressures (semi-isotropic, a coupling constant of 4.0 ps, a lateral reference pressure of −16 bar, and a compressibility of 3×10^{-5} bar^{-1} in the *x*–*y* plane and zero along the *z*-axis) were used to establish an *NPT* ensemble for equilibrium simulations. 200 ns separated MD simulations for different *x*–*y* scale systems were carried out using an *NVT* ensemble.

2.7 Statistical analysis

The data obtained were expressed as means ± SD (standard deviation). Statistical analysis was performed using Student's *t*-test for two groups and one-way analysis of variance for multiple groups. All experiments were conducted at least in triplicate.

3 Results and discussion

3.1 Characterization of sinapultide-loaded MBs at different concentrations

The construction of sinapultide loaded lipid MBs is illustrated in Fig. 2A. In this study, we first used film-dispersion and sonication methods to prepare a suspension of MBs, and then SF_6 was used as the filling gas to obtain sinapultide loaded MBs. Since both sinapultide and phospholipid components indicate superior biocompatibility, the sinapultide-based MBs can be potentially used for *in vivo* application. The hydrophobic sinapultide could be efficiently encapsulated in the MBs. When sinapultide concentrations in the prescription were 0.05, 0.1, 0.2, 0.4 and 0.8 mg mL^{-1}, the encapsulation efficiencies were 39.5 ± 2.1%, 46.3 ± 1.6%, 35.4 ± 0.9%, 21.3 ± 1.5%, and 15.6 ± 1.7%, respectively, and the LCs were 3.16 ± 0.3%, 3.67 ± 0.2%, 3.92 ± 0.4%, 4.33 ± 0.2%, and 4.79 ± 0.5%, respectively.

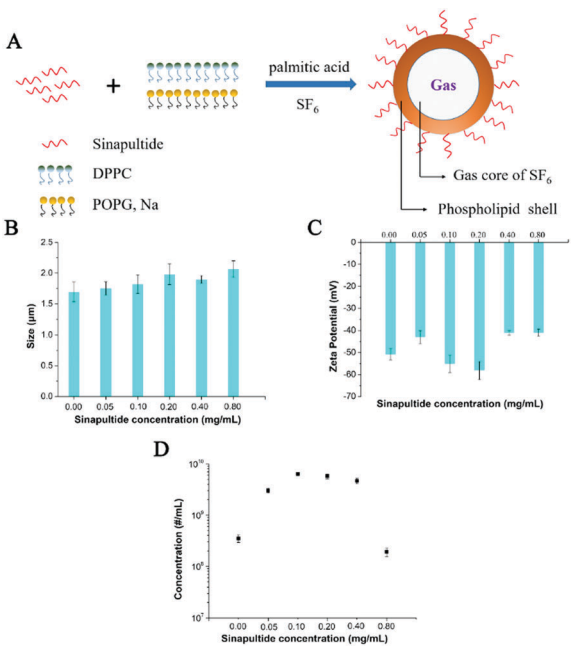

Fig. 2 (A) Schematic representation of the lipid microbubble with encapsulated sinapultide. (B) Mean diameters, (C) zeta potentials, and (D) microbubble yields of different formulations when the concentrations were set at 0.0, 0.05, 0.1, 0.2, 0.4 and 0.8 mg mL^{-1}.

Based on the fixed input amounts of gas and lipids, formulations with different concentrations of sinapultide were screened. The average sizes, zeta potentials, and concentrations of MBs were tested. Experimental results shown in Fig. 2B–D demonstrate that the optimal concentration of sinapultide was 0.1 mg mL^{-1}. With the optimized formulation, the sinapultide MBs have a mean diameter of 1.82 ± 0.15 μm, a zeta potential of −55.2 ± 3.9 mV, and a concentration of 6.37×10^9 MBs per mL. There was no significant difference in the diameters of the MBs with different concentrations of sinapultide. Therefore, it can be concluded that the sinapultide content changes will not significantly affect their sizes. Besides, the high negative charges of sinapultide loaded MBs can endow the MBs with good dispersion stability as proved in previous studies.[3] Furthermore, the stability of the sinapultide microbubble formulation was tested. The zeta potential, mean diameter, and microbubble yields were analyzed. The results showed that the mother liquor of the sinapultide suspension can retain good stability for 3 months (Fig. S1, ESI†).

Inverted microscopy images, TEM images, and LCSM images of sinapultide MBs, FITC labeled sinapultide MBs are shown in Fig. 3A–C, respectively. Fluorescence images of

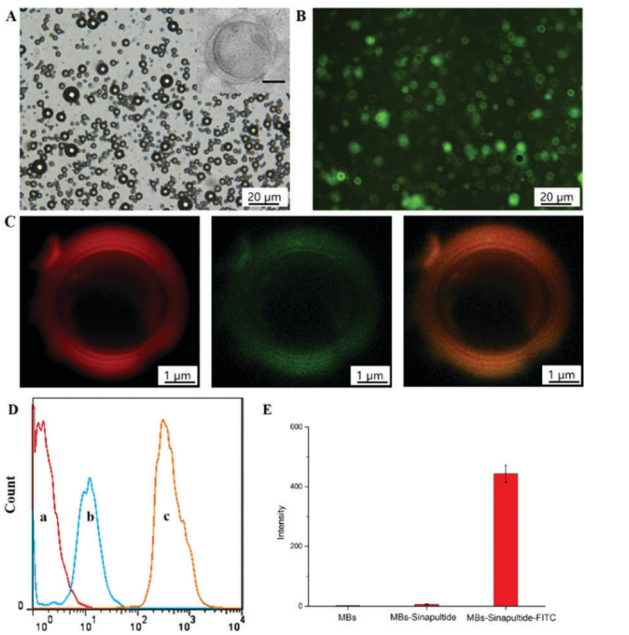

Fig. 3 Microscopy images of sinapultide (A) and FITC-labeled sinapultide-loaded lipid microbubbles (B) in bright fields. The inset in (A) shows the TEM image of microbubbles loaded with sinapultide, and the scale bar is 500 nm. (C) Laser Confocal Scanning Microscopy (LCSM) images of sinapultide-loaded lipid microbubbles with excitation wavelengths of 543 nm (in red color) and 488 nm (in green color), and the yellow picture is the fusion image. (D) Fluorescence intensity of microbubbles was analyzed using a flow cytometer. (a) Microbubbles without sinapultide, (b) sinapultide-loaded lipid microbubbles, and (c) FITC-labeled sinapultide-loaded lipid microbubbles. (E) Quantitative diagram of fluorescence intensity.

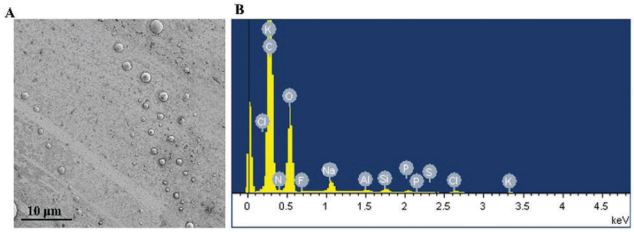

Fig. 4 SEM image showing the surface morphology of sinapultide-loaded lipid microbubbles (A) and elemental analysis of microbubbles (B).

FITC-labeled MBs showed that sinapultide was distributed in a lipid shell (Fig. 3B). In order to further quantitatively confirm that sinapultide was carried by the lipid layer successfully, the fluorescence intensity was tested using a flow cytometer. The results showed that sinapultide labelled by FITC indicated more than one hundred times of fluorescence intensity compared with non-sinapultide MBs, as shown in Fig. 3D and E. Moreover, SEM images and elemental analysis of sinapultide MBs are displayed in Fig. 4A and B. From the results of elemental analysis, we can see that nitrogen, sulfur, fluorine and other elements exist in sinapultide MBs.

3.2 Ultrasound imaging evaluation of sinapultide-loaded MBs *in vitro*

In vitro ultrasound imaging was performed using MBs coated with sinapultides at different concentrations. Since the dynamic behavior of MBs in an ultrasonic field was affected by the viscoelastic characteristics of their shells, which depends on the composition of the membrane shells to coated MBs,[49] the assembly of sinapultide onto the surface of the MBs at different concentrations may change the membrane shell's composition, structure and stability.[50] Thus, the signal in the US images may change with the increase of sinapultide concentration.

Fig. 5A shows the typical US images at 0, 5, 10, 15, 20 and 30 min after addition of different samples into the phantom. Acoustic imaging analysis *in vitro* indicated that ultrasound imaging enhancement could also be acquired by B-mode ultrasonography, as shown in Fig. S2 (ESI†). Furthermore, in order to study the effect of sinapultide concentration on the US enhancement effect, both the contrast mean power and the B-mode mean power were calculated quantitatively from the average grayscale values of the ROI of the images, which were recorded at 0, 5, 10, 15, 20 and 30 min. The plotted curves in Fig. 5B and C indicate that the US enhancement level and duration were related to the concentration of sinapultide. And the group of sinapultide MBs with 0.1 mg mL^{-1} has the brightest US image. The quantitative analysis according to Fig. 5A and D indicates that sinapultide loaded MBs maintain better US imaging enhancement within 30 min observation time except for the group of MBs with 0.8 mg mL^{-1} sinapultide. Based on US imaging, it is indicated that sinapultide MBs with 0.1 mg mL^{-1} concentration have the longest duration compared with the other groups and these optimized sinapultide MBs could last for more than 30 min *in vitro*. Thus this demonstrates the potential of their clinical application as contrast agents.[51–53]

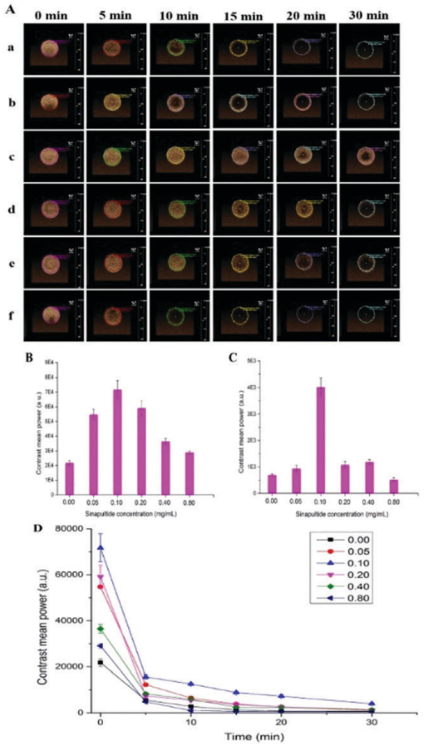

Fig. 5 *In vitro* ultrasonic evaluation of sinapultide-loaded lipid microbubbles. (A) The images of the six groups at different periods, and the formulations with different concentrations of sinapultide (0.0 (a), 0.05 (b), 0.10 (c), and 0.20 (d), 0.40 (e) and 0.80 (f) mg mL^{-1}). All samples were diluted 40 times. The B-mode mean power change of microbubbles after 0 min (B) and 30 min (C). Average mean contrast enhanced grayscale of US imaging of sinapultide microbubbles of different concentrations at different time courses (0, 5, 10, 15, 20, and 30 min) (D).

3.3 Stabilization mechanism of sinapultide MBs

In order to fully understand the stabilization mechanism of sinapultide for MBs, the simulation results in Fig. 6A show the distributions of 0, 2, 4, 8, 16, and 24 sinapultides on the lipid monolayer respectively. All of them lay parallel on the polar surface of the monolayer. A part of each peptide was wrapped by lipids. Each of them occupied a relatively independent space. It was hard to overlap with each other along the vertical direction. They steadily maintained a helical structure and a cylindrical shape. There was no apparent deformation though the system with 24 sinapultides was very crowded. The surface tension of the monolayer was calculated according to:[41]

$$\gamma_m = (P_N - P_L)\cdot L_z/2 \quad (3)$$

where P_N and L_z are the normal pressure and the size of the box. The lateral pressure P_L is the average of P_{xx} and P_{yy}. After *NPT* equilibrium simulations at a lateral reference pressure of −16 bar, we expanded the x and y of the box by 0.25 nm and performed 200 ns *NVT* simulation with each iteration until a pore formed on the monolayer. We calculated all the surface tensions at different areas of the monolayer. The surface tension–area profiles of monolayers for different numbers of sinapultides are shown in Fig. 6B. The surface tension increased as the area of

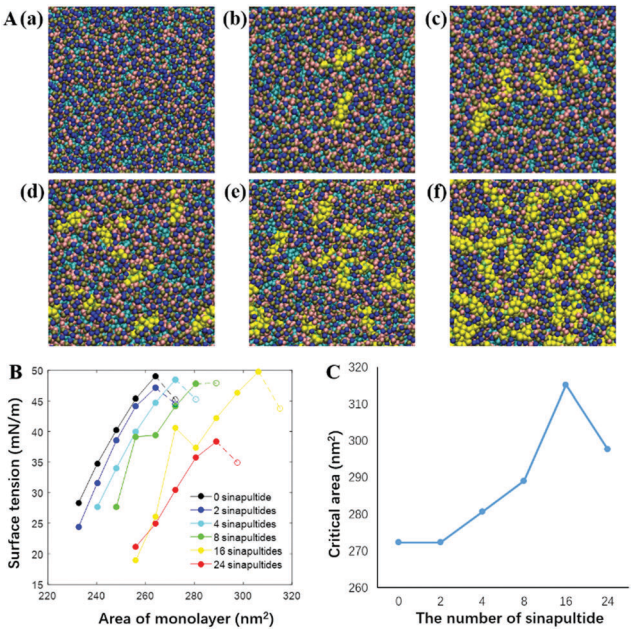

Fig. 6 (A) Overhead views of 0, 2, 4, 8, 16 and 24 sinapultides on the monolayers – snapshots (a–f) respectively. (B) The surface tension–area profiles of monolayers for different numbers of sinapultides. The end point of each profile was marked by a dashed line to illustrate the critical area where lipid pores formed initially. Black, blue, cyan, green, yellow and red colours were used to distinguish the 0, 2, 4, 8, 16 and 24 sinapultides on one monolayer respectively. (C) The plot of the number of sinapultides *vs.* critical area of the monolayer.

the monolayer enlarged during the first stage. The trend was similar to the results obtained in previous reports.[54] The right shift of the curve with the increase of sinapultide indicated that they could reduce the surface tension at the same area. This was consistent with SP-B, which could decrease the surface tension of pulmonary alveoli. It was also reported that the sinapultide spatial structure resembles an amphipathic domain of SP-B[47]. However, after the peak of the curve, the surface tension would decrease with an abnormally larger area indicated by a dashed line (end point) in Fig. 6B. It was because the monolayer ruptured and a pore formed at this point. We defined this area as the critical area and the surface tension as the critical surface tension corresponding to the last solid point, where the monolayer was about to rupture. These could be considered as the maximum area and surface tension that the system could be expanded to in a stable state.

More amounts of sinapultide induced larger critical areas when the number of sinapultides was less than 16, but the critical area decreased with 24 sinapultides on a monolayer, as shown in Fig. 6C. The results of simulations illustrated that the monolayer could be expanded to a larger area without breaking at a lower concentration of sinapultide, thus improving the stability of MBs efficiently. However, the overdose of sinapultide would result in the rupture of the monolayer at a smaller area. The two effects were very consistent with the inference in experiments. Besides, we observed that the critical surface tensions with 0–16 sinapultides were within the 46–50 mN m^{-1} range and the difference was very small in Fig. 6B. The right shift of the curve would lead to a larger critical area when the monolayer reached a similar critical surface tension with more sinapultide. In contrast, 24 sinapultides could also shift the curve to the right, but the critical surface tension was much less than those of 0–16 sinapultides. Therefore, the rupture occurred at a smaller area, and the stability of MBs decreased. The mechanism and experimental results also have the meaning of theory and practice for the preparation of other polypeptide MBs.

4 Conclusions

In this study, novel sinapultide stabilized MBs were developed by a film-ultrasonic method based on the phospholipid and synthetic lung surfactant formulation. By studying the structure and physicochemical properties of sinapultide MBs, it is found that appropriately sized MBs with regular morphological character could be prepared. The introduction of sinapultide does not significantly affect the size and zeta potential of the MBs. The *in vitro* ultrasound imaging evaluation demonstrated that the optimized sinapultide concentration (0.1 mg mL^{-1}) could maintain better stability and US imaging enhancement. Moreover, the results of molecular dynamics simulations show that the addition of sinapultide can efficiently decrease the surface tension to MBs. Accordingly, the stability of the MBs greatly improves. Compared with MBs prepared using animal-sourced pulmonary surfactants, MBs fabricated using the synthetic pulmonary surfactant sinapultide not only exhibit satisfactory immunogenicity but also exhibit good batch homogeneity.[32] Overall, synthetic lung surfactant microbubbles show promising clinical potential as an ultrasound contrast agent. It should be possible to use sinapultide MBs as a drug delivery system and as a potential theranostic agent in biomedical applications.[55,56]

Conflicts of interest

There are no conflicts to declare.

Acknowledgements

This work was supported by the National Key Research and Development Program of China (2017YFA0104302), the National Important Science Research Program of China (No. 2013CB733804), the National Natural Science Foundation of China for the Key Project of International Cooperation (61420106012), the National Natural Science Foundation of China (31370019), and the Center for Traditional Chinese Medicine R&D of West Anhui University and the Collaborative Innovation Center of Suzhou Nano Science and Technology. And the funding also partially came from the Six Talent Peaks Project of Jiangsu Province and Zhongying Young Scholars of Southeast University.

Notes and references

1 J. R. Lindner, *Nat. Rev. Drug Discovery*, 2004, **3**, 527–533.
2 Y. Jin, C. Jia, S.-W. Huang, M. O'Donnell and X. Gao, *Nat. Commun.*, 2010, **41**, 1–8.
3 L. Duan, F. Yang, W. He, L. Song, F. Qiu, N. Xu, L. Xu, Y. Zhang, Z. Hua and N. Gu, *Adv. Funct. Mater.*, 2016, **26**, 8313–8324.
4 Z. Xing, H. Ke, J. Wang, B. Zhao, X. Yue, Z. Dai and J. Liu, *Acta Biomater.*, 2010, **6**, 3542–3549.
5 F. Yang, M. Li, H. Cui, T. Wang, Z. Chen, L. Song, Z. Gu, Y. Zhang and N. Gu, *Sci. China Mater.*, 2015, **58**, 467–480.
6 J. Tian, F. Yang, H. Cui, Y. Zhou, X. Ruan and N. Gu, *ACS Appl. Mater. Interfaces*, 2015, **7**, 26579–26584.
7 X. Cai, F. Yang and N. Gu, *Theranostics*, 2012, **2**, 103–112.
8 A. G. Arranja, V. Pathak, T. Lammers and Y. Shi, *Pharmacol. Res.*, 2017, **115**, 87–95.
9 D. Liu, F. Yang, F. Xiong and N. Gu, *Theranostics*, 2016, **6**, 1306–1323.
10 F. Yang, M. Li, Y. Liu, T. Wang, Z. Feng, H. Cui and N. Gu, *J. Controlled Release*, 2016, **228**, 87–95.
11 E. Stride and M. Edirisinghe, *Soft Matter*, 2008, **4**, 2350–2359.
12 E. Stride and M. Edirisinghe, *Med. Biol. Eng. Comput.*, 2009, **47**, 883–892.
13 M. H. Lee, V. Prasad and D. Lee, *Langmuir*, 2009, **26**, 2227–2230.
14 J. Wan, A. Bick, M. Sullivan and H. A. Stone, *Adv. Mater.*, 2008, **20**, 3314–3318.
15 U. Farook, H. B. Zhang, M. J. Edirisinghe, E. Stride and N. Saffari, *Med. Eng. Phys.*, 2007, **29**, 749–754.
16 S. Tinkov, R. Bekeredjian, G. Winter and C. Coester, *J. Pharm. Sci.*, 2009, **98**, 1935–1961.
17 E. Unger, T. Porter, J. Lindner and P. Grayburn, *Adv. Drug Delivery Rev.*, 2014, **72**, 110–126.
18 S. Orsi, E. Di Maio, S. Iannace and P. A. Netti, *Nano Res.*, 2014, **7**, 1018–1026.
19 H. L. Liu, C. H. Fan, C. Y. Ting and C. K. Yeh, *Theranostics*, 2014, **4**, 432–444.
20 M. A. Borden, *Curr. Opin. Colloid Interface Sci.*, 2014, **19**, 480–489.
21 M. Lee, E. Y. Lee, D. Lee and B. J. Park, *Soft Matter*, 2015, **11**, 2067–2079.
22 Y. Y. Zuo, R. A. Veldhuizen, A. W. Neumann, N. O. Petersen and F. Possmayer, *Biochim. Biophys. Acta, Biomembr.*, 2008, **1778**, 1947–1977.
23 B. Piknova, V. Schram and S. Hall, *Curr. Opin. Struct. Biol.*, 2002, **12**, 487–494.
24 R. P. Valle, T. Wu and Y. Y. Zuo, *ACS Nano*, 2015, **9**, 5413–5421.
25 A. Hidalgo, A. Cruz and J. Pérez-Gil, *Eur. J. Pharm. Biopharm.*, 2015, **95**, 117–127.
26 P. Mikolka, D. Mokrá, J. Kopincová, L. Tomcikova-Mikusiakova and A. Calkovská, *Physiol. Res.*, 2013, **62**, S191.
27 O. Blanco and J. Pérez-Gil, *Eur. J. Pharmacol.*, 2007, **568**, 1–15.
28 B. T. Bloom, J. Kattwinkel, R. T. Hall, P. M. Delmore, E. A. Egan and W. A. Carlo, *Pediatrics*, 1997, **100**, 31–38.
29 T. E. Wiswell, G. R. Knight, N. N. Finer, S. M. Donn, H. Desai and T. A. Merritt, *Pediatrics*, 2002, **109**, 1081–1087.
30 R. E. Pattle, *Nature*, 1955, **175**, 1125–1126.
31 S. Sirsi, C. Pae, D. K. T. Oh, H. Blomback, A. Koubaa, B. Papahadjopoulos-Sternberg and M. Borden, *Soft Matter*, 2009, **5**, 4835–4842.
32 S. R. Sirsi, C. Fung, S. Garg, M. Y. Tianning, P. A. Mountford and M. A. Borden, *Theranostics*, 2013, **3**, 409–419.
33 R. H. Pfister and R. F. Soll, *Neonatology*, 2005, **87**, 338–344.
34 M. K. Lal and S. K. Sinha, *Ther. Adv. Respir. Dis.*, 2008, 339–344.
35 A. Katsnelson, *Nat. Biotechnol.*, 2012, **30**, 380.
36 O. Braide-Moncoeur, N. T. Tran and J. R. Long, *Curr. Opin. Chem. Biol.*, 2016, **32**, 22–28.
37 D. Liu, J. Xing, F. Xiong, F. Yang and N. Gu, *Drug Dev. Ind. Pharm.*, 2017, **43**, 652–660.
38 F. Yang, Y. Li, Z. Chen, Y. Zhang, J. Wu and N. Gu, *Biomaterials*, 2009, **30**, 3882–3890.
39 S. J. Marrink, A. H. de Vries and A. E. Mark, *J. Phys. Chem. B*, 2004, **108**, 750–760.
40 S. J. Marrink, H. J. Risselada, S. Yefimov, D. P. Tieleman and A. H. de Vries, *J. Phys. Chem. B*, 2007, **111**, 7812–7824.
41 C. Laing, S. Baoukina and D. P. Tieleman, *Phys. Chem. Chem. Phys.*, 2009, **11**, 1916–1922.
42 X. B. Lin, C. L. Wang, M. Wang, K. Fang and N. Gu, *J. Phys. Chem. C*, 2012, **116**, 17960–17968.
43 C. G. Cochrane and S. D. Revak, *Science*, 1991, **254**, 566–568.
44 D. H. de Jong, G. Singh, W. F. D. Bennett, C. Arnarez, T. A. Wassenaar, L. V. Schafer, X. Periole, D. P. Tieleman and S. J. Marrink, *J. Chem. Theory Comput.*, 2013, **9**, 687–697.
45 R. L. Thurlkill, G. R. Grimsley, J. M. Scholtz and C. N. Pace, *Protein Sci.*, 2006, **15**, 1214–1218.
46 M. Konishi, T. Fujiwara, T. Naito, Y. Takeuchi, Y. Ogawa, K. Inukai, M. Fujimura, H. Nakamura and T. Hashimoto, *Eur. J. Pediatr.*, 1988, **147**, 20–25.
47 C. G. Cochrane, *FEBS Lett.*, 1998, **430**, 424.
48 D. Van Der Spoel, E. Lindahl, B. Hess, G. Groenhof, A. E. Mark and H. J. Berendsen, *J. Comput. Chem.*, 2005, **26**, 1701–1718.
49 D. J. Park, K. H. Min, H. J. Lee, K. Kim, I. C. Kwon, S. Y. Jeong and S. C. Lee, *J. Mater. Chem. B*, 2016, **4**, 1219–1227.
50 L. Duan, F. Yang, L. Song, K. Fang, J. Tian, Y. Liang, M. Li, N. Xu, Z. Chen and Y. Zhang, *Soft Matter*, 2015, **11**, 5492–5500.
51 K. Ferrara and R. Pollard, *Annu. Rev. Biomed. Eng.*, 2007, **9**, 415–447.
52 C. I. De, E. Zagato, K. Braeckmans, Y. Luan, J. N. De and S. C. De Smedt, *J. Controlled Release*, 2015, **197**, 20–28.
53 C. H. Fan, Y. H. Cheng, C. Y. Ting, Y. J. Ho, P. H. Hsu, H. L. Liu and C. K. Yeh, *Theranostics*, 2016, **6**, 1542–1555.
54 S. Baoukina, L. Monticelli, S. J. Marrink and D. P. Tieleman, *Langmuir*, 2007, **23**, 12617–12623.
55 F. Kiessling, S. Fokong, J. Bzyl, W. Lederle, M. Palmowski and T. Lammers, *Adv. Drug Delivery Rev.*, 2014, **72**, 15–27.
56 A. Dasgupta, M. Liu, T. Ojha, G. Storm, F. Kiessling and T. Lammers, *Drug Discovery Today*, 2016, **20**, 41–48.